International Journal of Applied Earth Observation and Geoinformation 132 (2024) 104068

Contents lists available at ScienceDirect

International Journal of Applied Earth Observation and Geoinformation

journal homepage: www.elsevier.com/locate/jag

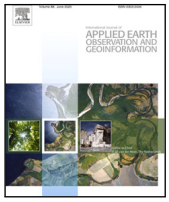

A spatio-temporal unmixing with heterogeneity model for the identification of remotely sensed MODIS aerosols: Exemplified by the case of Africa

Longshan Yang [a,1], Peng Luo [b,c,*,1], Zehua Zhang [d], Yongze Song [d,*], Kai Ren [d,e], Ce Zhang [f], Joseph Awange [h], Peter M. Atkinson [g,i], Liqiu Meng [b]

[a] Mining College, Guizhou University, Guiyang, China
[b] Chair of Cartography, Department of Aerospace and Geodesy, Technical University of Munich, Munich, Germany
[c] Senseable City Lab, Massachusetts Institute of Technology, Cambridge, USA
[d] School of Design and the Built Environment, Curtin University, Perth, Australia
[e] College of Natural Resources and Environment, Northwest A&F University, Yangling, Shaanxi 712100, China
[f] School of Geographical Sciences, University of Bristol, Bristol BS8 1SS, UK
[g] Lancaster Environment Centre, Lancaster University, Lancaster LA1 4YQ, UK
[h] School of Earth and Planetary Sciences, Spatial Science Discipline, Curtin University, Perth, Australia
[i] Geography and Environmental Sciences, University of Southampton, Highfield, Southampton SO17 1BJ, UK

ARTICLE INFO

Keywords:
Aerosol optical depth
Remote sensing
Spatio-temporal unmixing
Spatial heterogeneity
Africa

ABSTRACT

Aerosols are crucial constituents of the atmosphere, with significant impacts on air quality. Aerosol optical depth (AOD) is critical in assessing solar resources and modeling sky radiance. However, comprehensive aerosol studies at a continental scale are limited, and existing methodologies need to consider spatial characteristics. This study develops a spatio-temporal unmixing with heterogeneity (STUH) model to evaluate spatial patterns and temporal trends of atmospheric aerosols across the African continent. The spatio-temporal AOD data cube, comprising monthly averaged MODIS-derived AOD data from 2001 to 2015, was decomposed using spatially non-negative matrix variabilization to explore the spatial determinants and the impacts of their interactions to AOD using a geographically optimal zones-based heterogeneity (GOZH) model. Our findings reveal an increasing trend of aerosol levels across Africa in the past 15 years, combined with the spatio-temporal AOD pattern explained by five abundance variables. We find that in different regions across Africa, the impact of natural variables on AOD was 1.56 to 3.01 times the impact of human variables, with significant spatial variations. These results are essential for understanding the climatic implications of atmospheric aerosols in Africa.

1. Introduction

Atmospheric aerosols influence human health, climate change, and the use of solar energy (Li et al., 2020c; Wu et al., 2018). These microscopic suspended particles in ambient air comprise a variety of liquids and solids including, but not limited to dust, smoke from straw burning and solid dust from mining and quarrying processes (Haywood, 2021). The composition of aerosols has impacts on climate and human health. From a climatic risk perspective, aerosol particles can scatter and refract solar radiation, reducing the amount of solar radiation reaching the ground (Ramanathan et al., 2001; Ramanathan and Carmichael, 2008). Moreover, the size range of these particles is similar to the visible wavelengths, which affects the atmospheric extinction coefficient, leading to reduced visibility and impacting crop production (Bond et al., 2013; Gettelman et al., 2015). Furthermore, an increased concentration of cloud condensation nuclei can lead to a substantial rise in airborne lightning activity (Sun et al., 2021). In terms of human health risks, some aerosol particles pose hazards as these materials can attach to the respiratory tract or enter the alveoli and damage cellular DNA (Pope et al., 2011; Lelieveld et al., 2019). Studying aerosol composition and its explanatory variables is thus of great importance.

The explanatory variables behind atmospheric aerosols can be classified into anthropogenic and natural ones. Anthropogenic sources refer to human activities that emit various types of aerosol particles into the atmosphere, such as industrial $PM_{2.5}$ emissions and unburned fuel from

* Corresponding authors.
E-mail address: yongze.song@curtin.edu.au (Y. Song).
[1] These authors contributed equally to this work.

https://doi.org/10.1016/j.jag.2024.104068
Received 23 May 2024; Received in revised form 26 July 2024; Accepted 29 July 2024
Available online 2 August 2024

vehicles. Additionally, some human activities can increase solid particles, including crop waste burning, garbage burning, cigarette smoke, fireworks, and food cooking. On the other hand, natural variables, such as geographical location, climatic conditions, ecological state and wildfires can also affect the concentration and distribution of atmospheric aerosols. For example, surf-generated sea-salt and water vapor aerosols are major contributors to coastal zone concentrations (Tedeschi et al., 2017), while dust is the primary aerosol source in drought regions and deserts. Optical properties and seasonal variations in aerosols in China were investigated and shown that highly absorbing and non-absorbing aerosols occur seasonally (Chen et al., 2013). Moreover, ecological processes can change aerosol composition, such as when wildfires modify landscapes, alter surface albedo, and release greenhouse gases and aerosols into the atmosphere (Gunsch et al., 2018). However, as suggested by previous studies, the dynamic processes that lead to aerosol generation are complex, and determining the generating variables in some regions requires further research effort. Understanding the explanatory variables of aerosols is important for environmental protection and management.

In the current research, three statistical categories were used to identify the explanatory variables of geographical phenomenon: general spatial statistical analysis, spatio-temporal modeling, and machine learning (Song, 2022; Luo et al., 2023; Zhang et al., 2023; Song, 2023; Cheng et al., 2023). General spatial statistical analysis methods have been used widely to explore the influencing variables of aerosols. These methods include the Mann–Kendall mutation test (Zhang et al., 2021), spatial hotspot detection analysis (Amiridis et al., 2009), positive matrix variable analysis (Zhang et al., 2011), hierarchical cluster analysis (HCA) (Tutsak and Koçak, 2020), spatial autocorrelation analysis (Hua et al., 2016), trend analysis and wavelet analysis (Barik et al., 2020). However, the complexity of the aerosol mixing state and contribution leads to large uncertainties or biases in the study of chemical composition and anthropogenic contribution. Moreover, statistical analysis methods are not universally applicable to different study areas and do not always yield accurate results.

Spatio-temporal modeling has been proposed as a more comprehensive method of analyzing aerosols by considering their spatial and temporal characteristics. For example, the sectional aerosol model (CARMA) and the Community Earth System Model (CESM1) simulate aerosol microphysics, radiative properties, and interactions with clouds (Yu et al., 2015). Maximum Covariance Analysis (MCA) has been used to extract the variability of major aerosol regimes and allowed the simultaneous examination of aerosol variability both spatially and temporally (Li et al., 2014). However, spatio-temporal modeling methods cannot accurately model aerosol measurement data, and although modeling tools have advanced in the past two decades, including the evolution of the chemical mixing state of aerosols (Riemer et al., 2019), these models are not suitable for application to remote sensing data products to analyze the contribution and spatial properties of aerosols (Ma et al., 2018).

Recently, some researchers introduced machine learning in aerosol studies due to its ability to quickly and accurately acquire features from large-scale data (Chen et al., 2023). Transfer learning, for example, can significantly increase the accuracy of dust and cloud classification results by utilizing knowledge from previously collected data and adding dozens of new samples (Ma et al., 2015). Machine learning approaches such as neural networks and support vector machines can explore the reasons for persistent bias between the aerosol optical depths (AOD) retrieved from two measurements (Lary et al., 2009). However, the performance of machine learning methods can be limited by the number of labeled samples (Lary et al., 2009). Most machine learning methods are used to generate the AOD data instead of aerosol concentration analysis (Chen et al., 2020).

The above existing research methods have several limitations that this research aims to address. First, current approaches do not adequately consider the spatio-temporal characteristics of AOD data, particularly the local spatial homogeneity. Thus, spatio-temporal approaches need to be improved for a more effective understanding and analysis of aerosol dynamics. Second, previous methods have not effectively determined the impacts of individual variables and their interactions from a spatial perspective, which is crucial for a comprehensive understanding of aerosol sources and influences. To address the complexity of aerosol contributions, a few studies have presented Non-Negative Least Squares (NNLS) as a practical method for calculating aerosol compound composition and tracing the source of air pollution (McGraw, 2007; Gong et al., 2021). Finally, and most importantly, there is a significant lack of research focused on the entire African continent. To date, no study has investigated trends and classifications of aerosol types across the African continent. Only a few aerosol studies have focused on different regions of the African continent, such as the climatology of aerosol optical properties and aerosol emissions from savanna fires in South Africa (Andreae et al., 1998; Queface et al., 2011), and the impact of dust aerosol on regional precipitation and the importance of the diurnal cycle of AOD over western Africa (Solmon et al., 2008; Kocha et al., 2013). As a result, there is a substantial knowledge gap regarding aerosol dynamics in Africa.

In this research, we propose a Spatio-Temporal Unmixing with Heterogeneity (STUH) model to assess the spatial patterns and temporal trends in atmospheric aerosols across the African continent. Using the STUH model, we obtain the aerosol compound's spatio-temporal properties and analyze them alongside several natural and anthropogenic variables using the GOZH method. Consequently, this paper offers three significant contributions: (i) a novel method is developed to estimate aerosol types from a physical model perspective; (ii) the spatio-temporal characteristics of aerosols are determined; and (iii) a comprehensive study of atmospheric aerosols across Africa is conducted.

2. Spatio-temporal unmixing with heterogeneity model

2.1. Background: Concepts and methods of unmixing

Unmixing is a technique designed to decompose mixed signatures into a set of substance signatures and their corresponding proportions, demonstrating effectiveness in aerosols analysis (Wei and Wang, 2020). The success of unmixing relies on the mixing model, which describes how substances in a scene interact and form mixtures. As a result, unmixing can estimate parameters with physical meaning and facilitate mixture component analysis (Xu et al., 2015; Bhatia et al., 2018). Since atmospheric aerosols are mixtures, unmixing serves as a suitable method for analyzing aerosol compositions.

Unmixing methods can be classified into nonlinear and linear approaches (Borsoi et al., 2021). Nonlinear unmixing can describe substance mixing cases to a certain extent but may encounter limitations due to its complexity (Altmann et al., 2013; Li et al., 2020b). In contrast, linear spectral unmixing offers simplicity, high efficiency, and clear physical meaning, making it suitable for images with sub-meter spatial resolution (Wei and Wang, 2020). However, linear unmixing remains a challenging and ill-posed inverse problem due to the presence of observation noise, environmental conditions, and spectral variability (Feng et al., 2022). Currently, linear unmixing methods can be categorized into five groups: geometric methods, nonnegative matrix variabilization (NMF), archetypal analysis (AA), Bayesian method and sparse unmixing (SU) (Wei and Wang, 2020). Deep learning was increasingly applied to unmixing, leveraging the advantages of neural networks in processing large datasets and their robust ability to solve nonlinear problems (Rasti et al., 2021; Özdemir et al., 2022). These unmixing methods have the potential to facilitate more in-depth analysis of aerosols. In particular, NMF theory is used widely in unmixing due to its ability to preserve the non-negative properties of data (Feng et al., 2022).

2.2. Possible explanations of unmixing for spatio-temporal analysis

Initially developed for hyperspectral image processing, unmixing, also known as "spectral unmixing", was employed to address the challenges posed by mixed pixels with coarse spatial resolution in imaging spectrometers (Xu et al., 2018). Spectral unmixing decomposes the spectral signature of a mixed pixel into a set of pure substance spectral signatures, termed "endmembers", and their corresponding abundances. Hyperspectral image unmixing typically consists of two stages: endmember extraction and abundance estimation (Wang et al., 2022; Campos-Delgado et al., 2022).

Due to its ability to derive interpretable physical parameters, unmixing has been widely adopted in various research fields. In fluorescence measurements, overlapping fluorescence spectra are computationally separated using fluorescence unmixing (Ikoma et al., 2014). In medical multispectral optoacoustic tomography (MSOT), blind source unmixing methods were proposed to decompose the spectral contributions of different photo-absorbing molecules of interest in real-time, enabling the identification of tissue biomarkers (Zhang et al., 2020). For lunar surface mineral distribution analysis, unmixing of spectral reflectance data serves as an effective method for mineral resource interpretation, particularly in hard-to-access areas (Yin et al., 2019). In addition, unmixing is also used to analyze temporal social media data to detect land use patterns (Wu et al., 2020).

Unmixing was also utilized in spatio-temporal data analysis to explore the spatial characteristics and temporal trends of feature changes. From a field perspective, the applications of unmixing for spatio-temporal data analysis can be classified into three aspects. First, in the field of environmental monitoring, techniques such as time series analysis based on partial unmixing for vegetation were employed for soil remediation monitoring in coal mining regions, enabling fast and unbiased detection and extraction of single landcover classes of interest (Künzer et al., 2008). Similarly, Landsat time series data unmixing was utilized to assess spatial and temporal changes of urban vegetation at regional scales (Lu et al., 2017). The spatio-temporal spectral unmixing approach was also proposed for automatic dynamic monitoring of land cover changes, exploiting multi-scale spatio-temporal information and extracting proportion information from unchanged mixed pixels required for training (Wang et al., 2021).

Second, in urban areas, researchers used unmixing techniques on coarse-spatial-fine-temporal remote sensing data to predict time-series impervious surface maps (Chen et al., 2021; Knight and Voth, 2010). Furthermore, linear and nonlinear unmixing models were combined to extract impervious surfaces in nonshadow and shadow areas in medium-resolution images (Luo and Chen, 2021).

Finally, with the increasing availability of multitemporal data, the analysis of spatial properties and temporal trends has become increasingly significant in many research fields. Techniques such as empirical orthogonal function and temporal unmixing analysis were employed to monitor phenological characteristics and spatial distribution of vegetation using MODIS and EVI data (Xu and Fu, 2015). Additionally, crop-specific Normalized Difference Vegetation Index (NDVI) profiles were retrieved using two unmixing approaches from fine-resolution land-cover maps (Atzberger et al., 2014), followed by sub-pixel crop acreage estimation using non-linear unmixing of temporal information (Atzberger and Rembold, 2013).

Existing unmixing methods for spatio-temporal data analysis still exhibit limitations. First, these methods have difficulty in capturing the spatio-temporal characteristics of geospatial and Earth data due to local spatial homogeneity, resulting in a limited understanding of local data dynamics. In addition, these methods are not proficient in quantifying the impacts of individual variables and their interactions from both spatial pattern and spatial association perspectives.

2.3. The proposed model

In this paper, a spatio-temporal unmixing with heterogeneity (STUH) model is proposed to decompose the spatio-temporal data into temporal trends and spatial distribution characteristics, and determine the composition. It includes two basic elements: spatio-temporal cube generation and unmixing with the heterogeneity model. A few time series aerosol data are overlapped into an data cube in spatio-temporal cube generation step. Then, the aerosol data cube are analyzed for influence factors in unmixing with the heterogeneity model. At the final step, we conduct a sensitivity analysis to evaluate the uncertainty of the proposed method.

2.3.1. The generation of spatio-temporal cube

The temporal data of the response variables in the study area should be transformed into a spatio-temporal cube. In this study, the spatio-temporal data of aerosols are aggregated into images on a monthly base (t), where X and Y dimensions represent geographic location. The aerosol data of each month record the average aerosol level for that month. All aerosol data covering the same (x, y) region share the same location, and can be combined to represent a time series. In this way, at any given moment, the corresponding section can be achieved in the three-dimensional spatio-temporal cube.

2.3.2. Spatio-temporal unmixing with heterogeneity models

The spatial–temporal-unmixing-based model extracts the temporal trend and spatial variation in the composition aerosols through spatial homogeneous region segmentation and spatial–temporal unmixing. Spatial homogeneous region segmentation is utilized to acquire irregular subregions composed of homogeneous combinations of neighboring image elements by a named simple linear iteration clustering (SLIC) method. The spatial–temporal unmixing is implemented using the NMF method to decompose the endmembers and abundances, where the abundance can be considered as the spatial distribution of the components in the aerosol, and the endmember as the temporal trend of the components.

2.3.2.1. Spatial homogeneous region segmentation. The process can be viewed as grouping image pixels in space, and all pixels in the same homogeneous region are considered to be of the same sparsity to construct group sparsity constraints. Given the image $\boldsymbol{Y} \in \mathbb{R}^{T\times m\times n}$, in which m, n, T are the height, width and date, the SLIC approach is used to segment it with three steps as follows:

(1) Assignment of region centers

Assuming that the region number is K, the region seeds are sampled on a regular grid spaced $S = \sqrt{\frac{N}{K}}$ pixel apart. All pixels surrounded by the same seed are assigned the same region label.

(2) Similarity calculation

Setting a $2S \times 2S$ sized search window with the kth seed in the center, and calculating the similarity between this seed and all pixels in the window, the region label of the pixel is updated with the largest similarity value. The similarity calculation can be formulated as:

$$\begin{aligned} d_c &= \|y_k^0 - y_i\|_2 \\ d_s &= \sqrt{(m_k - m_i)^2 + (n_k - n_i)^2} \\ D_{ki} &= d_c + \frac{\kappa}{S} d_s \end{aligned} \tag{1}$$

where y_i and y_k^0 denote the ith pixel vector in the search window and the kth seed vector, respectively; m_k, n_k, m_i, and n_i are their spatial locations; d_c and d_s are their distance in vector and space, respectively; D_{ki} is the similarity, where a lower value means more similar; κ is a weight for balancing vector and spatial.

(3) Updating of region centers

After reassigning the region labels to each pixel, the corresponding region centers need to be re-defined by the following:

$$\hat{\mathbf{s}}_k = \frac{1}{N_k} \sum_{i \in G_k} \boldsymbol{g}_{ik} \tag{2}$$

where, $\hat{s}_k = [y_k, m_k, n_k]^T$ denotes the kth region center vector; G_k denotes the kth region with N_k pixels; g_{ik} denotes the vector of the ith pixel in the kth region. Then, step 2 and 3 are repeated until the predefined conditions are met.

2.3.2.2. Spatial–temporal unmixing. Since NMF could variablize a matrix $\boldsymbol{Y}$ into two smaller matrices $\boldsymbol{W} \in \mathbb{R}^{T\times K}$ and $\boldsymbol{H} \in \mathbb{R}^{K\times m\times n}$, with the k denotes the number of endmember and $\boldsymbol{Y} \approx \boldsymbol{W}\boldsymbol{H}$, in which all elements are non-negative, it enhances the interpretability of the matrix $\boldsymbol{Y}$ in various applications. To analyze the spatial pattern and temporal trend of the contributions of aerosol cross the entire study area, the temporal response variable (e.g. aerosol data in this study) need to be combined to form a spatio-temporal data cube. Local spatial homogeneity is an important spatial feature in aerosol data, and serves as a spatial constraint of the NMF method. Thus, the process is defined as spatial–temporal unmixing.

To solve an approximate decomposition with respect to $\boldsymbol{Y}$, the objective function is constructed based on the Euclidean distance between $\boldsymbol{Y}$ and $\boldsymbol{W}\boldsymbol{H}$, considering the local spatial homogeneity. The minimization of the objective function is denoted as:

$$\arg\min_{\boldsymbol{H}\boldsymbol{W}} \frac{1}{2}\|\boldsymbol{Y}-\boldsymbol{W}\boldsymbol{H}\|_{\mathrm{F}}^2+\alpha\sum_{s=1}^{N_s}\sum_{i\in\vartheta_s} c_i \left\|\boldsymbol{W}^s\boldsymbol{h}_i\right\|_2^2 \text{ s.t. } \boldsymbol{H}\geq 0, \boldsymbol{W}\geq 0, \boldsymbol{H}\boldsymbol{I}=\mathbf{1}^{\mathrm{T}} \tag{3}$$

where the operator$\|\cdot\|_F$ denotes the Frobenius norm; α adjusts the weights of the local spatial constraints, $\alpha \in (0, 1)$.

The projected gradient descent algorithm for non-negative matrix variabilization is used to calculate $\boldsymbol{W}$ and $\boldsymbol{H}$ in two steps alternately (Lin, 2007).

(1) Spatial feature extraction

In the first step, assuming that the endmember $\boldsymbol{W}$ is known, the abundance map $\boldsymbol{H}$ is created by.

$$\boldsymbol{H}^s = \max\left(0, \boldsymbol{H}^s - \alpha_k\left(\widetilde{\boldsymbol{W}}^T\left(\widetilde{\boldsymbol{W}}\boldsymbol{H}^s-\widetilde{\boldsymbol{Y}}^s\right)+\alpha\left(\boldsymbol{W}^s\right)^T\boldsymbol{W}^s\boldsymbol{H}^s\boldsymbol{B}^s\right)\right) \tag{4}$$

where $\widetilde{\boldsymbol{Y}}^s = \begin{bmatrix}\boldsymbol{Y}^s \\ \delta\mathbf{1}_{ns}\end{bmatrix}$, $\widetilde{\boldsymbol{W}} = \begin{bmatrix}\boldsymbol{W} \\ \delta\mathbf{1}_K\end{bmatrix}$.

(2) Temporal feature estimation

In the second step, the endmember $\boldsymbol{W}$ is updated by using the first step result—the abundance map $\boldsymbol{H}$.

$$\boldsymbol{W} = \max\left(0, \boldsymbol{W}-\beta_k(\boldsymbol{W}\boldsymbol{H}-\boldsymbol{Y})\boldsymbol{H}^T\right) \tag{5}$$

where α_k, β_k denote the step size.

2.3.2.3. GOZH-based explanatory variable identification. The spatial stratified heterogeneity model was employed to identify the explanatory variables of aerosols by analyzing the estimated abundance map. Spatial stratified heterogeneity involves comparing variance within strata, defined by geospatial variables, to those between strata (Wang et al., 2010, 2016). In recent years, several advanced methods were developed based on spatial stratified heterogeneity theory for geographical variable exploration and spatial prediction. These methods include optimal parameter-based geographical detectors (OPGD) (Song et al., 2020), interactive detectors for spatial association (IDSA) (Song and Wu, 2021), the generalized heterogeneity model (GHM) (Luo et al., 2023), robust geographical detectors (Zhang et al., 2022), geographically optimal zones-based heterogeneity (GOZH) (Luo et al., 2022), and locally explained stratified heterogeneity model (Li et al., 2023).

Among the above techniques, the GOZH model offers the advantage of avoiding underestimation and overestimation of spatial associations between geographical variables while providing fine-grained divisions of zones in geographical variable exploration (Luo et al., 2022). This model was implemented for investigating geographical variables related to soil moisture (Luo et al., 2021), carbon emissions (Wang et al., 2023) and public health issues (Tang et al., 2023). In this research, the GOZH model was employed to examine the potential explanatory variables of aerosols. The GOZH model uses a novel index, Ω, to characterize spatial stratified heterogeneity with high accuracy and robust performance (Wang et al., 2010; Luo et al., 2022; Song et al., 2020).

$$\Omega = \mathrm{Max}\left[1-\frac{SSW}{SST}\right] \tag{6}$$

where Ω is an indicator to measure spatial stratified heterogeneity, SSW is the sum of squares within subzones, and SST is the total sum of squares for marine chlorophyll across the entire study area. The Ω value is determined through a step-wise approach.

2.3.2.4. Identifying spatial varying relationships. The relationship between geographical variables exhibits spatial heterogeneity. Exploring the spatial variation of these relationships can deepen our understanding of geographical phenomena and help design appropriate actions and policies for different regions. The proposed STUH model can identify several abundances of response variable in space and explain the impact of explanatory variables on each abundance of the response variable. Since these abundances have spatial distribution details, the STUH model can thus calculate the spatial variation between response and explanatory variables.

For an explanatory variable i, its impact to the response variable at location j is calculated as follows:

$$\text{Abundance-based } \Omega(\mathrm{i})_j = \sum_{m=1}^{K} A(\mathrm{m})_j \Omega(\mathrm{i}) \tag{7}$$

where $A(\mathrm{m})_j$ is the abundance value of the mth endmember at the location j, K is the number of the endmembers, $\Omega(\mathrm{i})$ is the Ω value of the explanatory variable i.

2.3.3. Sensitivity analysis

In order to demonstrate the robustness of the model, we conducted a sensitivity analysis of the parameters. The number of endmembers is a crucial parameter in this research for aerosol component analysis. We set different numbers of endmembers and obtained results using the STUH model. The Ω values of the explanatory variables with varying endmember counts are calculated and compared to analyze the stability of the model results.

3. Study area and data

3.1. Study area

As one of the seven continents, Africa boasts a diverse and complex topography. The continent is endowed with an extensive variety and reserve of proven mineral resources, although their distribution is markedly uneven. Consequently, Africa's regional economic distribution pattern is characterized as "developed in the north and south, backward in the middle, rich in the north and south, poor in the middle". This unique landscape results in substantial aerosol presence with considerable spatial variability across the continent. Investigating African aerosols is therefore of critical importance for understanding their environmental implications across the continent.

3.2. AOD product datasets

According to solar radiation attenuation by atmosphere aerosol constituents, aerosol optical depth (AOD) can be retrieved from satellite remote sensing observation data for assessing the aerosol vertical column loading in ambient air (Bright and Gueymard, 2019; Filonchyk et al., 2019). AOD is a comprehensive parameter that has significantly improved our understanding of geographical aerosol properties (Filonchyk et al., 2019; He et al., 2021).

In this research, the AOD product (Remer et al., 2005) comes from the MODIS sensor, which is one of the most important sensors on the NASA Terra and Aqua satellites and has 36 spectral channels covering

Table 1
Explanatory variables of the spatial disparities of AOD.

Class	Variable	Dataset	Spatial resolution	Temporal resolution
Anthropogenic variables	Emission	SO_2 (EDGAR v5.0) BC (EDGAR v5.0) $PM_{2.5}$ (EDGAR v5.0) VOC (EDGAR v5.0) OC (EDGAR v5.0) NO_x (EDGAR v5.0)	0.1 degree	Annual
Natural variables	Vegetation	MOD13A1.006 NDVI MOD13A1.006 EVI	500 m	16-days
	Temperature	MOD11A2.006 LST	1200 m	8-days
	Precipitation	GPM v6	0.1 degree	Monthly

the UV, visible, NIR and IR wavelengths with fine spatial resolution. MODIS is a widely used aerosol detection sensor with high update frequency and wide spectral range. Its Level 2 $MOD04_{L2}$ AOD product datasets are available covering Africa from 2001–2015. The average value of effective image elements in the study area is calculated using pixels as the processing unit to obtain the monthly average AOD data for Africa.

3.3. Explanatory variables

In this study, we selected 10 explanatory variables to explain the spatial distributions of AOD in Africa. These include six emission-related variables, two vegetation-related variables, land surface temperature, and precipitation. The details of these explanatory variables are presented in Table 1.

Various air pollutants, generated by human activities, can directly or indirectly affect aerosol composition. To explore their influence, we collected six anthropogenic emission-related variables: NOx (Li et al., 2020a), PM2.5 (Just et al., 2018), black carbon (BC) (He et al., 2020), organic carbon (OC) (Levy et al., 2010), SO_2 (Mhawish et al., 2021), and VOC (Zhang et al., 2012). These annual emission data were sourced from the Emissions Database for Global Atmospheric Research (EDGAR), specifically the EDGARv5.0 product, which records emission values at a resolution of 0.1 x 0.1 degrees (Janssens-Maenhout et al., 2019).

The concentration and distribution of aerosols are deeply affected by natural changes and human activity. As part of nature, atmospheric aerosols interact with other components anytime and anywhere, such as climate and environment. In this study, to analyze the influence of natural sources in aerosols, three variables, NDVI (Mao et al., 2012), EVI (Obata et al., 2016) and LST (Pande et al., 2024), were used to exemplify the relationship between AOD spatio-temporal data and the three variables.

Both NDVI and EVI are vegetation indices, which highlight the characteristics of vegetation in remote sensing images and effectively reflect the ecological conditions. Thus, they are selected as the ecological variables in this research. NDVI can reflect background effects of the plant canopy, such as soil, wet ground, snow, dead leaves, roughness, etc. EVI can reduce the effects from both atmospheric and soil noise, and stabilize the response to vegetation. They are derived from the 16-days MOD13A1 composition with the spatial resolution of 500 m (Cheng et al., 2022). Land Surface Temperature (LST) is a fundamental aspect of climate and biology, determining the radiative energy budget of the Earth's surface and affecting organisms and ecosystems from local to global scales. Therefore, it is used as the climate environment variable in this study. We collected the temperature data from the 8-days MOD11A2 products (de Andrade et al., 2021). The precipitation process can not only remove aerosol particles, but also re-release them through evaporation, which can seriously affect the concentration and distribution of aerosols. In this study, we collected monthly precipitation data from the Global Precipitation Measurement (GPM) version 6. This dataset records precipitation values with a spatial resolution of 0.1 degrees (Moazami and Najafi, 2021).

4. Case study and results

4.1. Study workflow

The workflow of exploring the explanatory variables behind AOD across Africa using the STUH model is shown in Fig. 1. First, the AOD data and the remote sensing data products representing 10 explanatory variables were obtained and reprojected to a spatial resolution of 0.1° by means of mean synthesis (Fig. 1a). For the time series of 10 explanatory variables, the mean image and slope image were calculated, respectively. A total of 20 image datasets were obtained. Second, for the time series products of AOD, a mixed pixel decomposition was performed (Fig. 1b). In this study, we determined that the number of endmembers should be set at five. This decision was made based on a visual check of the unmixing results. We will substantiate the rationality of this choice through comprehensive sensitivity analysis. Third, for the 10 explanatory variables, the spatial pattern and temporal pattern were revealed (Fig. 1c).3 Fourth, for the five endmembers of AOD, the GOZH model was used to calculate the determinant power of each variable ((Fig. 1d)). The determining power is the synergistic effect of mean and slope. In addition, we explored the determinants of human and natural variables on the five endmembers. Finally, a sensitivity analysis was applied to the abundance numbers (Fig. 1e). In this study, the number of endmembers was set to range from 3 to 6.

4.2. Spatio-temporal pattern of AOD and explanatory variables across Africa

Fig. 2(a) show the annual averaged values of AOD during 2001–2015. Over this time, AOD has significantly increased (β value = 1.16) in these regions: rapid urbanization and industrialization activities took place, and these activities may result in considerable anthropogenic aerosol emissions. Since ADRETOA and ADRESFC were all negative, the aerosols exerted cooling effects at the top of the atmosphere and the surface. However, there was a warming effect of aerosols within the atmosphere. The spatial distributions of ADRE were consistent with those of AOD.

The African continent was geographically divided into five regions, and their respective mean values and variances for aerosol optical depth (AOD) are shown in Fig. 2(b) and (c). The largest AOD values are observed in the western region (0.327), which is primarily covered by the Sahara desert with only one side facing the sea. On the other hand, the southern region is characterized by its mountainous terrain, numerous rivers, with three sides facing the sea, and produced the smallest AOD values (0.119). The statistical distributions of AOD values in the northern and eastern regions of Africa are similar, with average values of 0.214 and 0.203, respectively.

The geographical distribution of the 15-year averaged AOD over the continent of Africa is shown in Fig. 2(d). The largest AOD (1.168) occurred over and north of Chad, which is Tibesti Plateau, located in the middle of the Sahara Desert and composed of a series of volcanoes. It has high temperatures and little rainfall. The second largest AOD

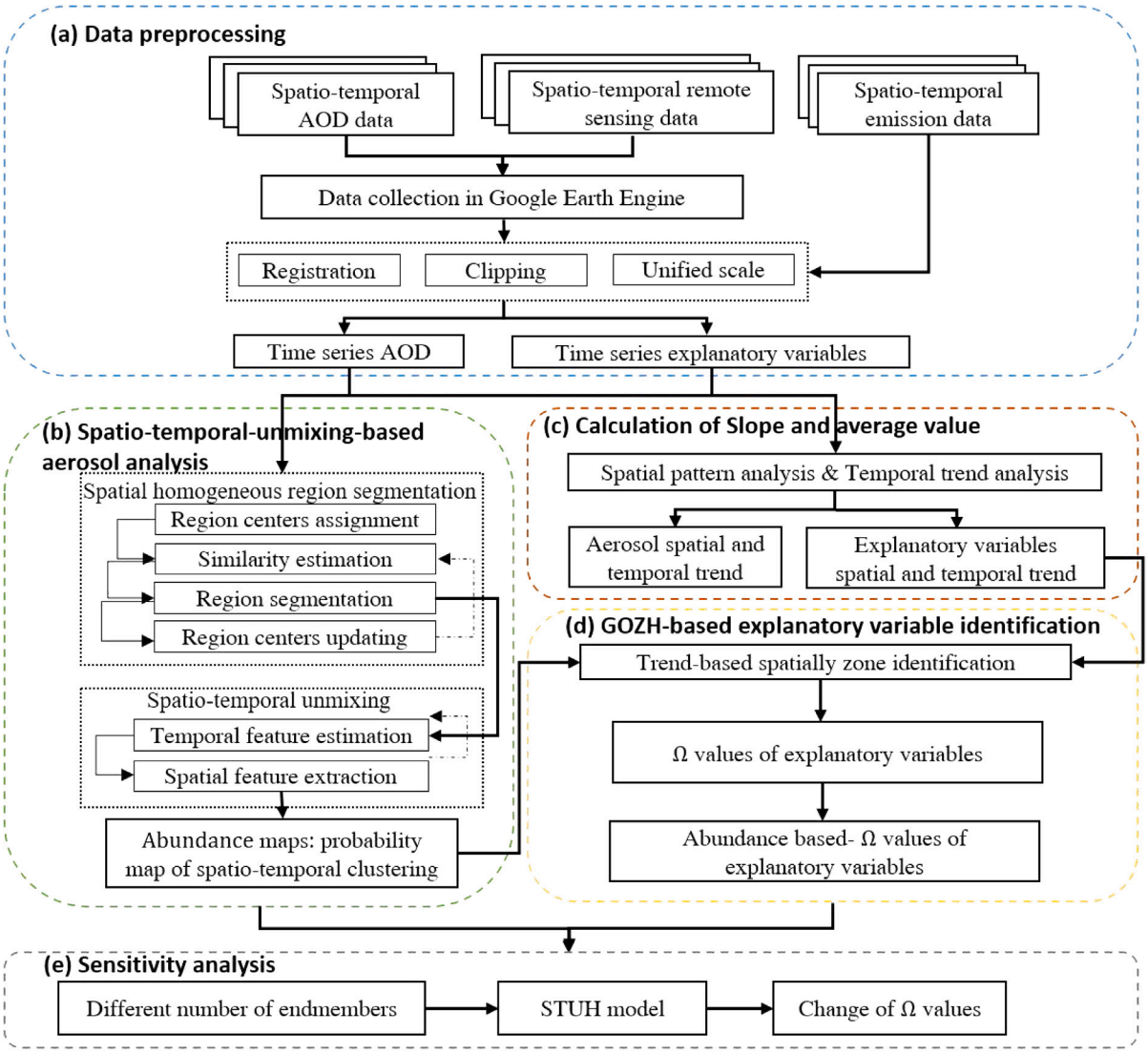

Fig. 1. Flowchart of spatio-temporal unmixing with heterogeneity (STUH)-based aerosol optical depths (AOD) analysis. The proposed STUH model is the combination of step b, c, and d.

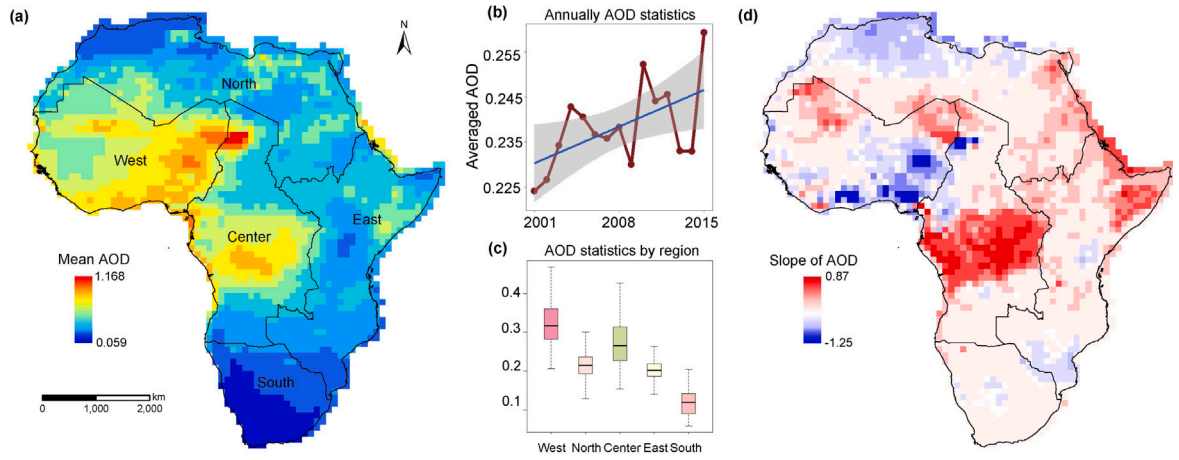

Fig. 2. Spatial and temporal statistics on African AOD. (a) Spatial distribution of annual average AOD; (b) temporal trends of AOD by year; (c) AOD statistics by region; and (d) spatial distribution of AOD slope.

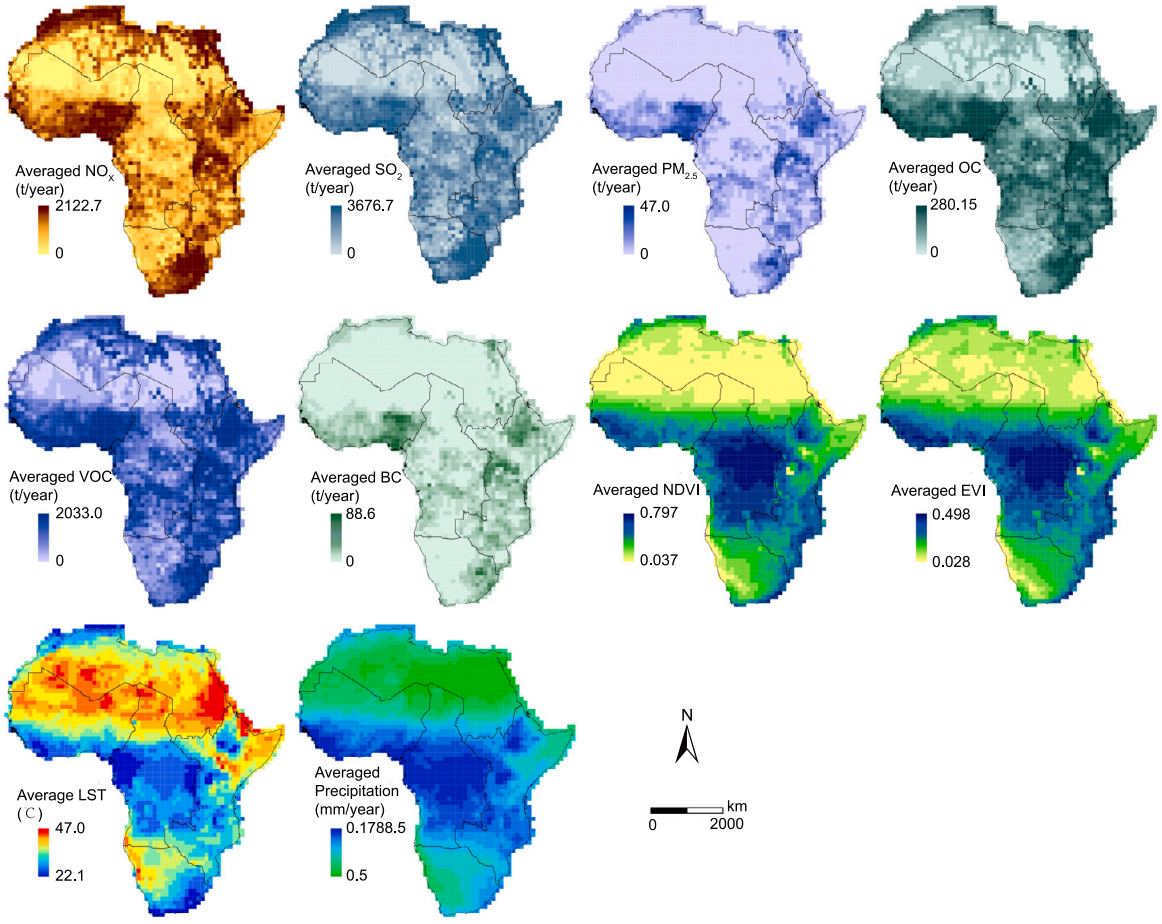

Fig. 3. Spatial patterns of explanatory variables presented by the annual average values over 15 years: NO_x, SO_2, $PM_{2.5}$, OC, VOC, BC, NDVI, EVI, LST, and precipitation.

levels occurred mainly in the marginal areas, namely, Porto Novo, Libreville, Lomé, and so on. Large AOD values were closely related to coarse-particle aerosol and attributable to large amounts of airborne dust and sand rising from the natural surface of the eastern coastal area. In the other high AOD areas, located mainly in lowland and densely populated areas, the large amounts of fine-particle aerosols from anthropogenic activities occupied a larger proportion of the total aerosols. Large emissions of coarse-particle aerosols, such as soot and dust aerosols originating from industrial pollution and civil coal fuel combustion, were another important source.

To identify the overall trend across the entire continent, a long-term linear trend analysis based on the slope of AOD over Africa was undertaken (Fig. 2(e)). In the Gulf of Guinea coastal countries, as well as in parts of Chad, AOD showed a decreasing trend. This may indicate an environmental improvement from 2001 to 2015. However, in central African regions, such as the Democratic Republic of Congo, the slope of change in AOD is close to 0.5, showing a more pronounced upward trend.

The spatial pattern of the explanatory variables related to aerosols is also presented in Fig. 3. These variables were increasing across continent and have a strong global consistency. The mean values of most explanatory variables are smaller in North Africa and part of South Africa and larger in Central Africa. The opposite is true for some other variables. For example LST is larger in the North and lower in Central Africa. This is because North Africa is dominated by the Sahara desert and the South Africa by the basin area. In the South African highlands in the south, each various variable is lower than other regions. The range of averaged natural variable values is larger than for anthropogenic variables. Comparing natural variables with anthropogenic variables, the latter has a more apparent spatial pattern than the former. In general, the spatial pattern of most explanatory variables is positively related to AOD and negatively associated with LST.

Fig. 4 shows the temporal trends of the various explanatory variables. The temporal trends of natural explanatory variables are similar, especially in Africa's central and southern regions. These natural explanatory variables change less in the northern Sahara Desert region and slightly more variable in the south and central areas. The temporal trends for NO_x and SO_2 are consistent, with minor variation across the continent and only a tiny number of significant shifts, such as in Cairo, Pretoria, Accra, Takoradi. The temporal trends of the $PM_{2.5}$, OC, VOC and BCD variables are strongly similar, and their range of variation is slightly more than that of the first two variables, for example, in Nigeria.

4.3. STUH-based variables affecting AOD patterns

To analyze the relationship between aerosols and various potential influencing variables on the African continent, the AOD was decomposed using the STUH method to determine five endmembers, and the spatial distribution characteristics of each endmembers were obtained.

Determining the geographical area corresponding to each abundance is the first analysis to be performed. It can be seen from these five spatial distribution characteristics that the different endmembers have obvious spatial aggregation characteristics (Fig. 5). Abundance 1 is mainly distributed in Central Africa. In Central Africa it has an average value of 0.190, while in other regions it is 0.002 to 0.104. Abundance 2 was mainly distributed in humid subtropical climate regions in Central

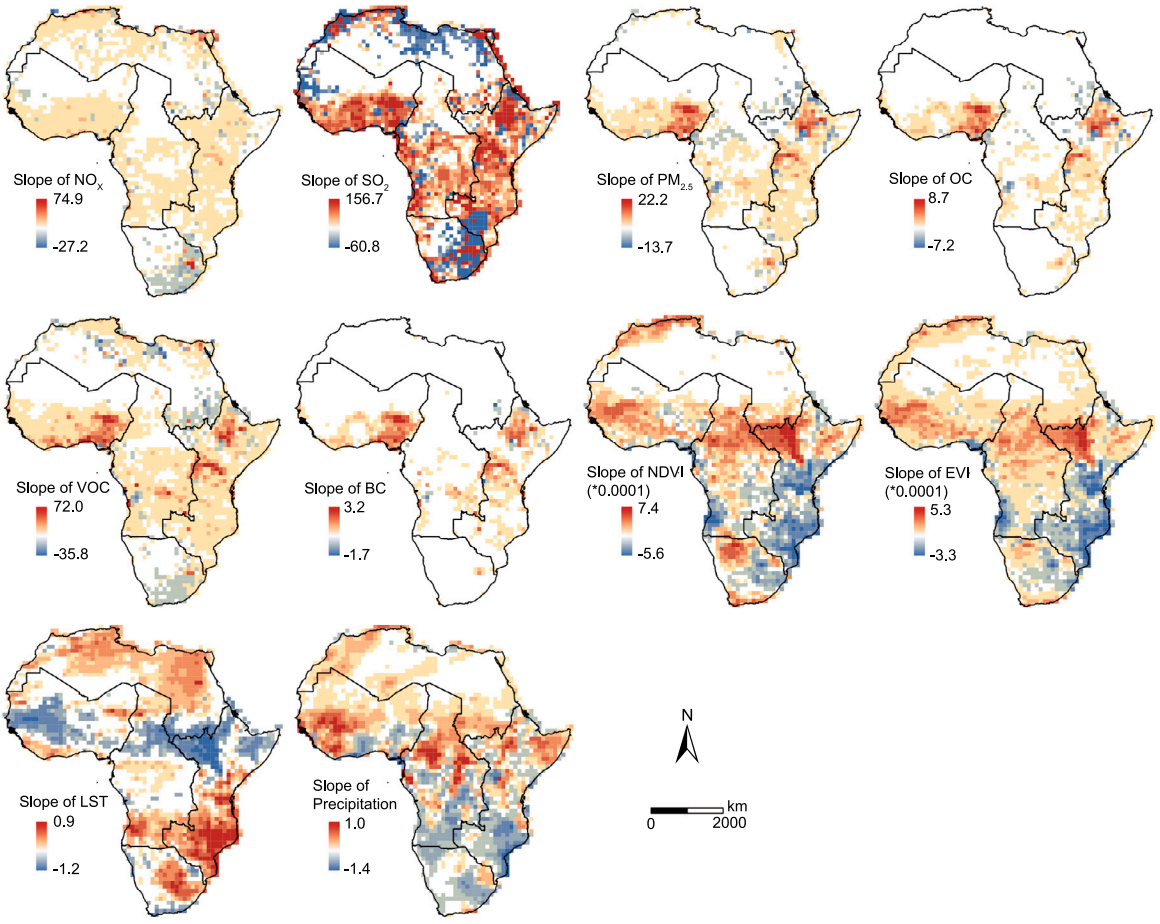

Fig. 4. Temporal patterns of explanatory variables presented by the slope of annual values among 15 years: NO_x, SO_2, $PM_{2.5}$, OC, VOC, BC, NDVI, EVI, LST, and precipitation.

and Southern Africa (b). Abundance 3 has a large number of outliers, especially for the Central African region. It is mainly distributed in the Tibesti Mountains. Among all the abundances, abundance 4 has the widest spatial distribution with larger values. This suggests that abundance 4 characterizes the main explanatory variables of AOD in Africa. Among them, the value of abundance 4 is the largest in North Africa and the lowest in Central Africa. Abundance 5 is mainly distributed in densely populated Western Africa (e).

Once the geographical areas corresponding to the abundances are determined, the explanatory variables of AOD in each area can be analyzed. The determinants of each abundances were developed by the GOZH model. The average value and slope of each variable were fed to the GOZH model to obtain its contribution to AOD. Results show that the power of determinant (Ω) of human and natural variables are critically different among the five regions.

In abundance 1, natural variables are much more critical than human variables. The Ω value ranges from 0.258 to 0.339 for the four natural variables, and the Ω value ranges from 0.026 to 0.058 for the human variables. This shows that the AOD in this area is less influenced by humans. In abundance 2, the influence of natural variables on AOD is still much greater than that of human variables. However, the gap between the two is reduced compared to abundance 1. Among them, EVI was the most important explanatory variables (Ω = 0.485, $P < 0.05$), which indicates that vegetation in this region had the greatest impact on AOD. Abundance 3 is mainly concentrated in the northern mountainous area, and the explanatory variables analysis shows that the contributions of natural variables and human variables to AOD are demonstrating that the causes of AOD are complex. Of these, temperature is the most important explanatory variables (Ω = 0.265). Abundance 4 is the most widely distributed type. Environmental and natural variables also have the strongest explanatory power for AOD. Among them, the Ω value range of human elements is from 0.129 to 0.268, and the Ω value range of environmental elements is from 0.365 to 0.623. NDVI and EVI, two variables representing vegetation, had the greatest impact on AOD. This shows that the lack of vegetation is the main explanatory variable in most of northern Africa, as well as in South Africa. Abundance 5 is found in more densely populated areas. Rainfall was the most important spatial determinant of AOD, followed by vegetation. Among human variables, OC emissions had the greatest impact on AOD (Ω = 0.258).

For the spatial pattern of different potential variables, the variance plot shows that the influence of abundance 4 has the largest value and the largest range of values, followed by abundance 2, and the smallest one is abundance 3, also the most concentrated. This indicates that the degree of influence of natural variables and anthropogenic variables on AOD differed greatly in endmembers 4 and 2, while the influence of these two variables was relatively small in endmember 3.

All the variables including the average values and slopes were merged into a single natural variable and human variable. They were input to the GOZH model to explore the overall effect of human and environment variables on AOD. In general, the natural variable is always larger than the anthropogenic variable in each abundance. Fig. 5(f) shows that the natural impact is about 1.564–3.010 times greater than the human impact on AOD, which varies in different regions. This indicates that the aerosols in the African continent are mostly influenced by natural variables.

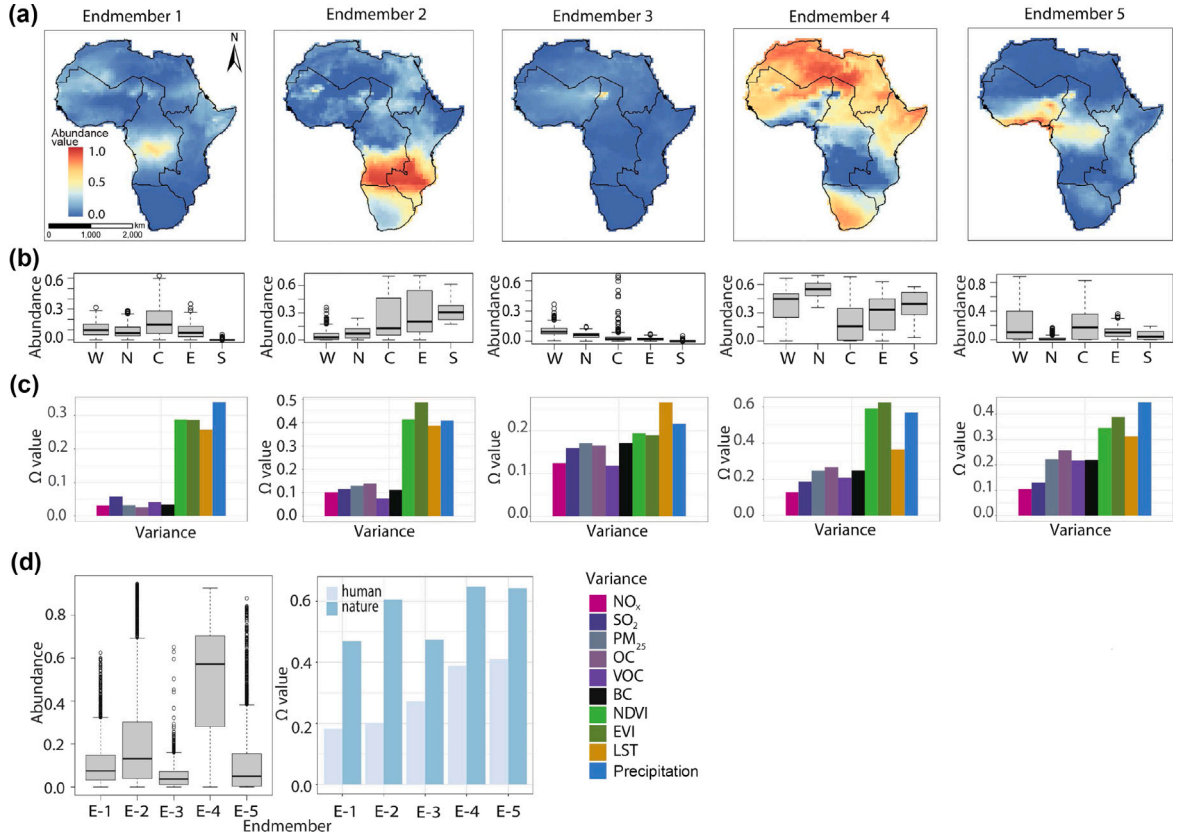

Fig. 5. A matrix on statistical summaries of five endmembers. (a) Abundance maps; (b) statistical summaries of abundance by regions; (c) Ω values of explanatory variables for the abundances; and (d) summaries of abundances and Ω values for five endmembers.

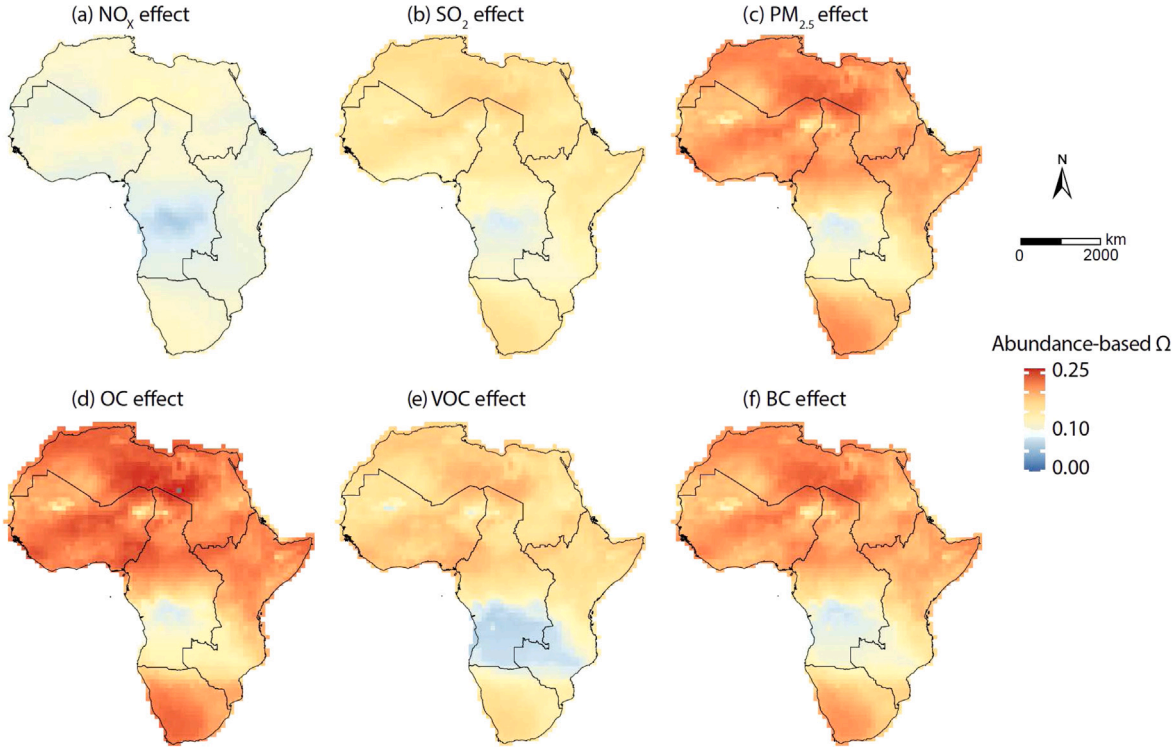

Fig. 6. Spatial distributions of impacts of different human variables on AOD quantified using the abundance-based Ω, including impacts of (a) NO_x, (b) SO_2, (c) $PM_2.5$, (d) OC, (e) VOC, and (f) BC.

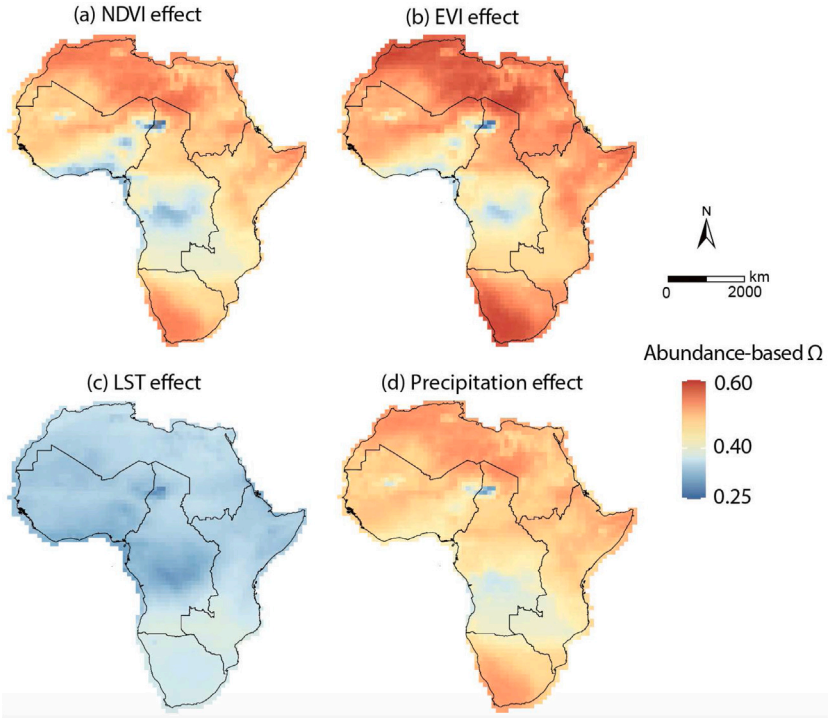

Fig. 7. Spatial distributions of impacts of different natural variables on AOD quantified using the abundance-based Ω, including impacts of (a) NDVI, (b) EVI, (c) LST, and (d) precipitation.

4.4. The impact of human and environment variables on AOD

After calculating the Ω value for each explanatory variable and determining the abundance value of the AOD, we explored the abundance-based Ω values using Eq. (7).

The spatial effects of individual variables on AOD are revealed. Fig. 6 shows the abundance-based Ω value of six human variables. Results indicate that the spatial characteristics of these six anthropogenic influences have strong similarities, with the least influence in the south-central region of Africa and varying degrees of influence in other large areas. OC has the greatest impact on the spatio-temporal variation of AOD among human variables. In comparison, NO_x has the least impact, and $PM_{2.5}$ and BC have the most consistent impact.

The spatial distribution of Ω of natural variables was calculated (Fig. 7). In general, these four natural variables also have consistency in spatial distribution, all showing a small bias in the central local range and a large bias in different degrees in other regions. This is particularly evident in the most northern and southern regions. However, the influence of these four natural variables is the smallest in one region, but the AOD in that region is relatively high. Comparing the influencing variables with each other, it can be seen that these 4 influencing variables are EVI, NDVI, Precipitation and LST in the order from largest to smallest.

4.5. Sensitivity analysis

A sensitivity analysis was conducted to explore the influence of endmember numbers on the results. Fig. 8 shows the statistical results of Ω values for each influencing variable at different abundance numbers (3 to 6). The number of abundances in the STUH model determines the number of influencing variables and their corresponding spatial patterns of influence. The mean and slope of the Ω values also support this view (Fig. 8c). For the anthropogenic and natural variables, respectively, the Ω values for anthropogenic variables do not differ significantly for abundance numbers 4 and 5, but natural variables are significant for abundance numbers 5. The results indicate that five is the best abundance number for unmixing the time series AOD images in Africa.

Table 2
Comparison of functions between the developed spatio-temporal unmixing with heterogeneity (STUH) model and previous spatio-temporal models, including hierarchical cluster analysis (HCA), empirical orthogonal function (EOF), and transfer learning.

Model characteristics	HCA	EOF	Transfer learning	STUH model
Result expandability	✗	✓	✗	✓
Modeling nonlinearity	✗	✗	✓	✓
Temporal heterogeneity	✗	✓	✓	✓
Spatial heterogeneity	✗	✗	✗	✓

5. Discussion

5.1. Model comparison

To further analyze the characteristics of STUH method, we chose three existing methods together for comparative analysis, which are hierarchical cluster analysis (HCA) (Tutsak and Koçak, 2020), Empirical Orthogonal Function (EOF) (Xu et al., 2017) and transfer learning (Ma et al., 2015), as shown in Table 2. We analyze each method in four aspects, namely expandability, nonlinear, temporal heterogeneity, spatial heterogeneity and complexity. Compared with other methods, the STUH method had all properties. The transfer learning could handle the nonlinear aerosol data with high computational complexity and requires labeled samples, but it is difficult to explain the physical meaning of AOD variables and simultaneously analyze several aerosol variables. EOF did well in expandability and temporal heterogeneity. The HCA method is the only method with low complexity.

Aerosols have long plagued environmental protection and human health. Exploring the complex determinants behind them is crucial for environmental protection. However, most current methods use statistical analysis models that fail to consider the temporal and spatial heterogeneity of the explanatory variables. Hybrid image element decomposition methods can effectively classify hyperspectral images and have started to be applied to Spatio-temporal data analysis problems. In this research, we developed a model based on spatio-temporal hybrid

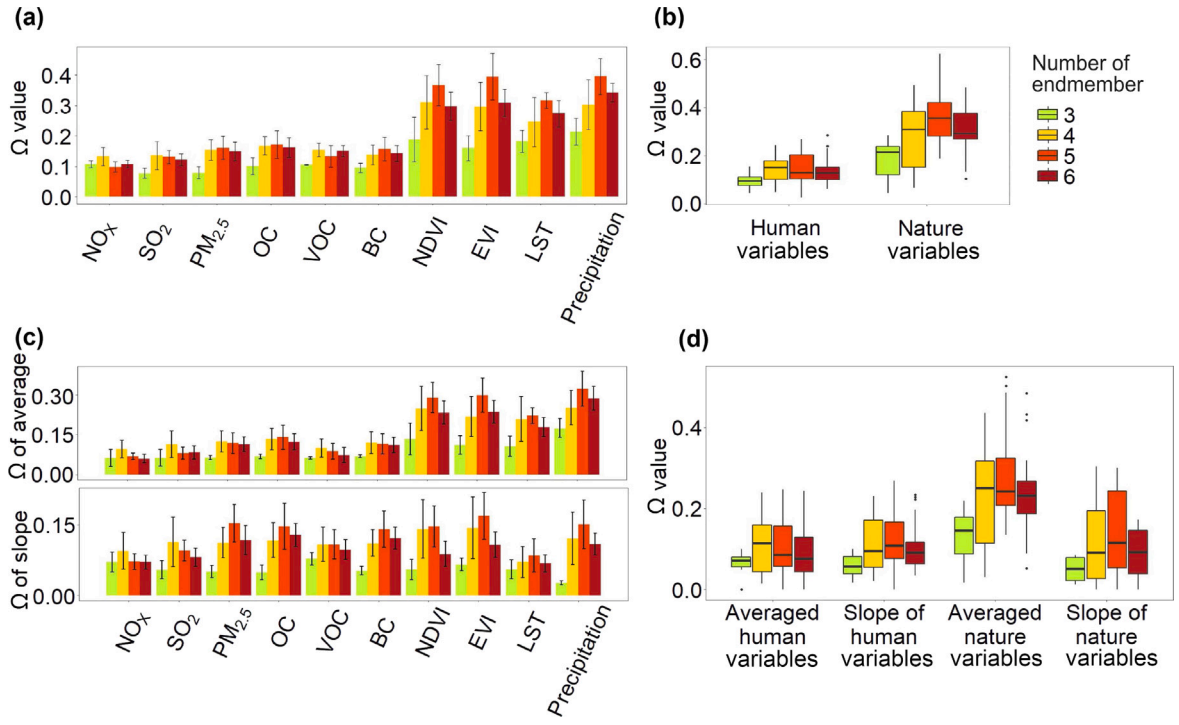

Fig. 8. Sensitivity analysis based on different explanatory variables and numbers of endmember.(a) Ω value for explanatory variables; (b) Ω value for natural and anthropogenic variables; (c) Ω value statistics for explanatory variables; (d) Ω value statistics for natural and anthropogenic variables.

image element decomposition to obtain the abundance of images characterizing the drivers by hybrid image element decomposition of long time series of aerosol data. Based on the local spatial homogeneity, a STUH model was proposed, to unmix the spatio-temporal AOD cube data by the NMF method for exploiting the variable patterns. After that, the GOZH model was introduced to interpret each abundance image interpretively. The resulting determinants of aerosol were thus determined.

5.2. Africa AOD analysis

In this research, we applied the proposed STUH method to analyze AOD of the Africa continent and achieved the following discoveries: First, by analyzing the variables influencing aerosols, we conclude that the influence of natural environmental variables is 1.5 to 3 times greater than the influence of anthropogenic variables in 2000–2015. Second, the proposed STUH method effectively separates anthropogenic and natural factors. For example, aerosols in the Gulf of Guinea region are mainly influenced by anthropogenic variables, due to the large population and industry. This result could be achieved for endmember 5 and was consistent with the results reported by several authors (Aklesso et al., 2018; Boiyo et al., 2017). Third, aerosols are most severe in the Sahara region during 2000–2015, shown in endmember 3 and endmember 4. This finding is consistent with the results reported by authors (Iguchi et al., 2018). But, endmember 3 shown the main influence by LST, and endmember 4 displayed the other natural variables.

This research offers new insights for analyzing spatio-temporal data and further complements its modeling theory. It contributes to the relatively sparse literature on AOD in Africa. The results provide an evidence base for local decision-making and government policy formulation across Africa, including by Ministries of Health.

6. Conclusion

This research investigated the spatial pattern and temporal trends of AOD during 2000–2015. We proposed an STUH model to explore the natural and anthropogenic variables influencing changes in AOD. The investigation of the spatial and temporal trends of AOD showed a significant increase. The overall spatial distribution of aerosols in Africa was distinctly localized and gradually increased due to natural environmental variability and anthropogenic variables. To analyze the causes of the increase in detail, the STUH model was used to unmix the AOD spatial and temporal matrix. The Ω values between each influencing variable and the abundance map were calculated using the GOZH model. The statistical results showed that for the African region, the influence of natural variables was more significant than that of anthropogenic variables, and the Enhanced Vegetation Index and the Organic Emission are the most influential natural and anthropogenic variables, respectively. This study provides a scientific solution to analyze the causes of aerosols, provides some reference for subsequent aerosol inversion studies, and provides guidance for aerosol research in Africa.

CRediT authorship contribution statement

Longshan Yang: Writing – original draft, Methodology, Formal analysis, Conceptualization. **Peng Luo:** Writing – original draft, Methodology, Investigation, Conceptualization. **Zehua Zhang:** Writing – review & editing, Visualization. **Yongze Song:** Writing – original draft, Supervision, Funding acquisition, Conceptualization. **Kai Ren:** Writing – review & editing. **Ce Zhang:** Writing – review & editing. **Joseph Awange:** Writing – review & editing, Investigation. **Peter M. Atkinson:** Writing – review & editing. **Liqiu Meng:** Writing – review & editing, Supervision.

Declaration of competing interest

The authors declare that they have no known competing financial interests or personal relationships that could have appeared to influence the work reported in this paper.

Data availability

Data will be made available on request.

Acknowledgments

This work was supported in part of funding from Curtin University, in part of National Natural Science Foundation of China 42301440, in part by Guizhou Provincial Science and Technology Projects [2022]133.

References

Aklesso, M., Kumar, K.R., Bu, L., Boiyo, R., 2018. Analysis of spatial–temporal heterogeneity in remotely sensed aerosol properties observed during 2005–2015 over three countries along the gulf of guinea coast in southern West Africa. Atmos. Environ. 182, 313–324.

Altmann, Y., Dobigeon, N., McLaughlin, S., Tourneret, J.-Y., 2013. Nonlinear spectral unmixing of hyperspectral images using gaussian processes. IEEE Trans. Signal Process. 61 (10), 2442–2453.

Amiridis, V., Balis, D., Giannakaki, E., Stohl, A., Kazadzis, S., Koukouli, M., Zanis, P., 2009. Optical characteristics of biomass burning aerosols over southeastern europe determined from uv-raman lidar measurements. Atmos. Chem. Phys. 9 (7), 2431–2440.

Andreae, M., Andreae, T., Annegarn, H., Beer, J., Cachier, H., Le Canut, P., Elbert, W., Maenhaut, W., Salma, I., Wienhold, F., et al., 1998. Airborne studies of aerosol emissions from savanna fires in Southern Africa: 2. Aerosol chemical composition. J. Geophys. Res.: Atmos. 103 (D24), 32119–32128.

Atzberger, C., Formaggio, A., Shimabukuro, Y., Udelhoven, T., Mattiuzzi, M., Sanchez, G., Arai, E., 2014. Obtaining crop-specific time profiles of ndvi: the use of unmixing approaches for serving the continuity between spot-vgt and proba-v time series. Int. J. Remote Sens. 35 (7), 2615–2638.

Atzberger, C., Rembold, F., 2013. Mapping the spatial distribution of winter crops at sub-pixel level using avhrr ndvi time series and neural nets. Remote Sens. 5 (3), 1335–1354.

Barik, G., Acharya, P., Maiti, A., Gayen, B.K., Bar, S., Sarkar, A., 2020. A synergy of linear model and wavelet analysis towards space–time characterization of aerosol optical depth (aod) during pre-monsoon season (2007–2016) over indian sub-continent. J. Atmos. Sol.-Terr. Phys. 211, 105478.

Bhatia, N., Iordache, M.-D., Stein, A., Reusen, I., Tolpekin, V.A., 2018. Propagation of uncertainty in atmospheric parameters to hyperspectral unmixing. Remote Sens. Environ. 204, 472–484.

Boiyo, R., Kumar, K.R., Zhao, T., Bao, Y., 2017. Climatological analysis of aerosol optical properties over East Africa observed from space-borne sensors during 2001–2015. Atmos. Environ. 152, 298–313.

Bond, T.C., Doherty, S.J., Fahey, D.W., Forster, P.M., Berntsen, T., DeAngelo, B.J., Flanner, M.G., Ghan, S., Kärcher, B., Koch, D., et al., 2013. Bounding the role of black carbon in the climate system: A scientific assessment. J. Geophys. Res.: Atmos. 118 (11), 5380–5552.

Borsoi, R.A., Imbiriba, T., Bermudez, J.C.M., Richard, C., Chanussot, J., Drumetz, L., Tourneret, J.-Y., Zare, A., Jutten, C., 2021. Spectral variability in hyperspectral data unmixing: A comprehensive review. IEEE Geosci. Remote Sens. Mag. 9 (4), 223–270.

Bright, J.M., Gueymard, C.A., 2019. Climate-specific and global validation of modis aqua and terra aerosol optical depth at 452 aeronet stations. Sol. Energy 183, 594–605.

Campos-Delgado, D.U., Cruz-Guerrero, I.A., Mendoza-Chavarría, J.N., Mejía-Rodríguez, A.R., Ortega, S., Fabelo, H., Callico, G.M., 2022. Nonlinear extended blind end-member and abundance extraction for hyperspectral images. Signal Process. 201, 108718.

Chen, H., Gu, X., Cheng, T., Li, Z., Yu, T., 2013. The spatial–temporal variations in optical properties of atmosphere aerosols derived from aeronet dataset over China. Meteorol. Atmos. Phys. 122 (1), 65–73.

Chen, R., Li, X., Zhang, Y., Zhou, P., Wang, Y., Shi, L., Jiang, L., Ling, F., Du, Y., 2021. Spatiotemporal continuous impervious surface mapping by fusion of landsat time series data and google earth imagery. Remote Sens. 13 (12), 2409.

Chen, W., Ran, H., Cao, X., Wang, J., Teng, D., Chen, J., Zheng, X., 2020. Estimating pm2. 5 with high-resolution 1-km aod data and an improved machine learning model over Shenzhen, China. Sci. Total Environ. 746, 141093.

Chen, A., Yang, J., He, Y., Yuan, Q., Li, Z., Zhu, L., 2023. High spatiotemporal resolution estimation of aod from himawari-8 using an ensemble machine learning gap-filling method. Sci. Total Environ. 857, 159673.

Cheng, Y., Zhang, L., Zhang, Z., Li, X., Wang, H., Xi, X., 2022. Spatiotemporal variation and influence factors of vegetation cover in the yellow river basin (1982–2021) based on gimms ndvi and mod13a1. Water 14 (20), 3274.

Cheng, T., Zhao, Y., Song, Y., Ma, L., Zhang, Z., Luo, P., Gao, P., Zhang, M., Zhao, C., 2023. Towards resilience effectiveness: Assessing its patterns and determinants to identify optimal geographic zones. J. Clean. Prod. 429, 139596.

de Andrade, M.D., Delgado, R.C., da Costa de Menezes, S.J.M., de Ávila Rodrigues, R., Teodoro, P.E., da Silva Junior, C.A., Pereira, M.G., 2021. Evaluation of the mod11a2 product for canopy temperature monitoring in the Brazilian atlantic forest. Environ. Monit. Assess. 193, 1–20.

Feng, X.-R., Li, H.-C., Wang, R., Du, Q., Jia, X., Plaza, A.J., 2022. Hyperspectral unmixing based on nonnegative matrix factorization: A comprehensive review. IEEE J. Sel. Top. Appl. Earth Obs. Remote Sens..

Filonchyk, M., Yan, H., Zhang, Z., Yang, S., Li, W., Li, Y., 2019. Combined use of satellite and surface observations to study aerosol optical depth in different regions of China. Sci. Rep. 9 (1), 1–15.

Gettelman, A., Shindell, D., Lamarque, J., 2015. Impact of aerosol radiative effects on 2000–2010 surface temperatures. Clim. Dyn. 45 (7), 2165–2179.

Gong, C., Xin, J., Wang, Y., Zhao, C., Yan, P., Wen, T., Song, T., Yang, Z., 2021. The contribution of aerosols chemical components to aerosol optical depth: The method and the case in dunhuang. Atmos. Res. 258, 105652.

Gunsch, M.J., May, N.W., Wen, M., Bottenus, C.L., Gardner, D.J., VanReken, T.M., Bertman, S.B., Hopke, P.K., Ault, A.P., Pratt, K.A., 2018. Ubiquitous influence of wildfire emissions and secondary organic aerosol on summertime atmospheric aerosol in the forested great lakes region. Atmos. Chem. Phys. 18 (5), 3701–3715.

Haywood, J., 2021. Atmospheric aerosols and their role in climate change. In: Climate Change. Elsevier, pp. 645–659.

He, L., Wang, L., Huang, B., Wei, J., Zhou, Z., Zhong, Y., 2020. Anthropogenic and meteorological drivers of 1980–2016 trend in aerosol optical and radiative properties over the yangtze river basin. Atmos. Environ. 223, 117–188.

He, Y., Xu, X., Gu, Z., Chen, X., Li, Y., Fan, S., 2021. Vertical distribution characteristics of aerosol particles over the guanzhong plain. Atmos. Environ. 255, 118444.

Hua, W., Junfeng, Z., Fubao, Z., Weiwei, Z., 2016. Analysis of spatial pattern of aerosol optical depth and affecting factors using spatial autocorrelation and spatial autoregressive model. Environ. Earth Sci. 75, 1–17.

Iguchi, T., Matsui, T., Tao, Z., Kim, D., Ichoku, C.M., Ellison, L., Wang, J., 2018. Nu-wrf aerosol transport simulation over West Africa: Effects of biomass burning on smoke aerosol distribution. J. Appl. Meteorol. Climatol. 57 (7), 1551–1573.

Ikoma, H., Heshmat, B., Wetzstein, G., Raskar, R., 2014. Attenuation-corrected fluorescence spectra unmixing for spectroscopy and microscopy. Opt. Express 22 (16), 19469–19483.

Janssens-Maenhout, G., Crippa, M., Guizzardi, D., Muntean, M., Schaaf, E., Dentener, F., Bergamaschi, P., Pagliari, V., Olivier, J.G., Peters, J.A., et al., 2019. Edgar v4. 3.2 global atlas of the three major greenhouse gas emissions for the period 1970–2012. Earth Syst. Sci. Data 11 (3), 959–1002.

Just, A.C., De Carli, M.M., Shtein, A., Dorman, M., Lyapustin, A., Kloog, I., 2018. Correcting measurement error in satellite aerosol optical depth with machine learning for modeling pm2. 5 in the northeastern usa. Remote Sens. 10 (5), 803.

Knight, J., Voth, M., 2010. Mapping impervious cover using multi-temporal modis ndvi data. IEEE J. Sel. Top. Appl. Earth Obs. Remote Sens. 4 (2), 303–309.

Kocha, C., Tulet, P., Lafore, J.-P., Flamant, C., 2013. The importance of the diurnal cycle of aerosol optical depth in West Africa. Geophys. Res. Lett. 40 (4), 785–790.

Künzer, C., Bachmann, M., Mueller, A., Lieckfeld, L., Wagner, W., 2008. Partial unmixing as a tool for single surface class detection and time series analysis. Int. J. Remote Sens. 29 (11), 3233–3255.

Lary, D.J., Remer, L., MacNeill, D., Roscoe, B., Paradise, S., 2009. Machine learning and bias correction of modis aerosol optical depth. IEEE Geosci. Remote Sens. Lett. 6 (4), 694–698.

Lelieveld, J., Klingmüller, K., Pozzer, A., Burnett, R., Haines, A., Ramanathan, V., 2019. Effects of fossil fuel and total anthropogenic emission removal on public health and climate. Proc. Natl. Acad. Sci. 116 (15), 7192–7197.

Levy, R., Remer, L., Kleidman, R., Mattoo, S., Ichoku, C., Kahn, R., Eck, T., 2010. Global evaluation of the collection 5 modis dark-target aerosol products over land. Atmos. Chem. Phys. 10 (21), 10399–10420.

Li, J., Carlson, B.E., Lacis, A.A., 2014. Application of spectral analysis techniques in the intercomparison of aerosol data. Part II: Using maximum covariance analysis to effectively compare spatiotemporal variability of satellite and aeronet measured aerosol optical depth. J. Geophys. Res.: Atmos. 119 (1), 153–166.

Li, L., Lu, C., Chan, P.-W., Zhang, X., Yang, H.-L., Lan, Z.-J., Zhang, W.-H., Liu, Y.-W., Pan, L., Zhang, L., 2020a. Tower observed vertical distribution of pm2.5, o3 and nox in the pearl river delta. Atmos. Environ. 220, 117083.

Li, Y., Luo, P., Song, Y., Zhang, L., Qu, Y., Hou, Z., 2023. A locally explained heterogeneity model for examining wetland disparity. Int. J. Digit. Earth 16 (2), 4533–4552.

Li, X., Mauzerall, D.L., Bergin, M.H., 2020c. Global reduction of solar power generation efficiency due to aerosols and panel soiling. Nat. Sustain. 3 (9), 720–727.

Li, M., Zhu, F., Guo, A.J., 2020b. A robust multilinear mixing model with l 2 1norm for unmixing hyperspectral images. In: 2020 IEEE International Conference on Visual Communications and Image Processing. VCIP, IEEE, pp. 193–196.

Lin, C.-J., 2007. Projected gradient methods for nonnegative matrix factorization. Neural Comput. 19 (10), 2756–2779.

Lu, Y., Coops, N.C., Hermosilla, T., 2017. Estimating urban vegetation fraction across 25 cities in pan-pacific using landsat time series data. ISPRS J. Photogramm. Remote Sens. 126, 11–23.

Luo, H., Chen, N., 2021. A combined unmixing framework for impervious surface mapping on medium-resolution images with visible shadows. Photogramm. Eng. Remote Sens. 87 (6), 431–443.

Luo, P., Song, Y., Huang, X., Ma, H., et al., 2022. Identifying determinants of spatio-temporal disparities in soil moisture of the northern hemisphere using a geographically optimal zones-based heterogeneity model. ISPRS J. Photogramm. Remote Sens. 185, 111–128.

Luo, P., Song, Y., Wu, P., 2021. Spatial disparities in trade-offs: economic and environmental impacts of road infrastructure on continental level. GISci. Remote Sens..

Luo, P., Song, Y., Zhu, D., Cheng, J., Meng, L., 2023. A generalized heterogeneity model for spatial interpolation. Int. J. Geogr. Inf. Sci. 37 (3), 634–659.

Ma, Y., Gong, W., Mao, F., 2015. Transfer learning used to analyze the dynamic evolution of the dust aerosol. J. Quant. Spectrosc. Radiat. Transfer 153, 119–130.

Ma, J., Zhang, W., Marinoni, A., Gao, L., Zhang, B., 2018. An improved spatial and temporal reflectance unmixing model to synthesize time series of landsat-like images. Remote Sens. 10 (9), 1388.

Mao, D., Wang, Z., Luo, L., Ren, C., 2012. Integrating avhrr and modis data to monitor ndvi changes and their relationships with climatic parameters in Northeast China. Int. J. Appl. Earth Obs. Geoinf. 18, 528–536.

McGraw, R., 2007. Numerical advection of correlated tracers: preserving particle size/composition moment sequences during transport of aerosol mixtures. In: Journal of Physics: Conference Series. Vol. 78, IOP Publishing, 012045.

Mhawish, A., Sorek-Hamer, M., Chatfield, R., Banerjee, T., Bilal, M., Kumar, M., Sarangi, C., Franklin, M., Chau, K., Garay, M., et al., 2021. Aerosol characteristics from earth observation systems: A comprehensive investigation over south asia (2000–2019). Remote Sens. Environ. 259, 112410.

Moazami, S., Najafi, M., 2021. A comprehensive evaluation of gpm-imerg v06 and mrms with hourly ground-based precipitation observations across canada. J. Hydrol. 594, 125929.

Obata, K., Miura, T., Yoshioka, H., Huete, A.R., Vargas, M., 2016. Spectral cross-calibration of viirs enhanced vegetation index with modis: A case study using year-long global data. Remote Sens. 8 (1), 34.

Özdemir, O.B., Koz, A., Yardımcı Çetin, Y., 2022. Non-linear hyperspectral unmixing with 3d convolutional encoders. Int. J. Remote Sens. 43 (9), 3236–3257.

Pande, C.B., Egbueri, J.C., Costache, R., Sidek, L.M., Wang, Q., Alshehri, F., Din, N.M., Gautam, V.K., Pal, S.C., 2024. Predictive modeling of land surface temperature (lst) based on landsat-8 satellite data and machine learning models for sustainable development. J. Clean. Prod. 444, 141035.

Pope, III, C.A., Burnett, R.T., Turner, M.C., Cohen, A., Krewski, D., Jerrett, M., Gapstur, S.M., Thun, M.J., 2011. Lung cancer and cardiovascular disease mortality associated with ambient air pollution and cigarette smoke: shape of the exposure–response relationships. Environ. Health Perspect. 119 (11), 1616–1621.

Queface, A.J., Piketh, S.J., Eck, T.F., Tsay, S.-C., Mavume, A.F., 2011. Climatology of aerosol optical properties in Southern Africa. Atmos. Environ. 45 (17), 2910–2921.

Ramanathan, V., Carmichael, G., 2008. Global and regional climate changes due to black carbon. Nat. Geosci. 1 (4), 221–227.

Ramanathan, V., Crutzen, P., Kiehl, J., Rosenfeld, D., 2001. Aerosols, climate, and the hydrological cycle. Science 294 (5549), 2119–2124.

Rasti, B., Koirala, B., Scheunders, P., Ghamisi, P., 2021. Undip: Hyperspectral unmixing using deep image prior. IEEE Trans. Geosci. Remote Sens. 60, 1–15.

Remer, L.A., Kaufman, Y., Tanré, D., Mattoo, S., Chu, D., Martins, J.V., Li, R.-R., Ichoku, C., Levy, R., Kleidman, R., et al., 2005. The modis aerosol algorithm, products, and validation. J. Atmos. Sci. 62 (4), 947–973.

Riemer, N., Ault, A., West, M., Craig, R., Curtis, J., 2019. Aerosol mixing state: Measurements, modeling, and impacts. Rev. Geophys. 57 (2), 187–249.

Solmon, F., Mallet, M., Elguindi, N., Giorgi, F., Zakey, A., Konaré, A., 2008. Dust aerosol impact on regional precipitation over Western Africa, mechanisms and sensitivity to absorption properties. Geophys. Res. Lett. 35 (24).

Song, Y., 2022. The second dimension of spatial association. Int. J. Appl. Earth Obs. Geoinf. 111, 102834.

Song, Y., 2023. Geographically optimal similarity. Math. Geosci. 55 (3), 295–320.

Song, Y., Wang, J., Ge, Y., Xu, C., 2020. An optimal parameters-based geographical detector model enhances geographic characteristics of explanatory variables for spatial heterogeneity analysis: Cases with different types of spatial data. GISci. Remote Sens. 57 (5), 593–610.

Song, Y., Wu, P., 2021. An interactive detector for spatial associations. Int. J. Geogr. Inf. Sci..

Sun, M., Liu, D., Qie, X., Mansell, E.R., Yair, Y., Fierro, A.O., Yuan, S., Chen, Z., Wang, D., 2021. Aerosol effects on electrification and lightning discharges in a multicell thunderstorm simulated by the wrf-elec model. Atmos. Chem. Phys. 21 (18), 14141–14158.

Tang, Y., Song, Y., Wang, Y., Lai, S., Alegana, V.A., Liu, X., 2023. National variation in patterns of bone disease treatment-seeking behaviors: A study of more than 50 000hospital admissions between 2008 and 2021. Int. J. Appl. Earth Obs. Geoinf. 117, 103219.

Tedeschi, G., Van Eijk, A.M.J., Piazzola, J., Kusmierczyk-Michulec, J.T., 2017. Influence of the surf zone on the marine aerosol concentration in a coastal area. Bound.-Layer Meteorol. 163 (2), 1–24.

Tutsak, E., Koçak, M., 2020. Optical and microphysical properties of the columnar aerosol burden over the eastern mediterranean: Discrimination of aerosol types. Atmos. Environ. 229, 117463.

Wang, Q., Ding, X., Tong, X., Atkinson, P.M., 2021. Spatio-temporal spectral unmixing of time-series images. Remote Sens. Environ. 259, 112407.

Wang, J., Li, X., Christakos, G., Liao, Y., Zhang, W., Gu, X., Zheng, X., 2010. Geographical detectors-based health risk assessment and its application in the neural tube defects study of the Heshun Region, China. Int. J. Geogr. Inf. Sci. 24 (1), 107–127.

Wang, Z., Li, J., Liu, Y., Xie, F., Li, P., 2022. An adaptive surrogate-assisted endmember extraction framework based on intelligent optimization algorithms for hyperspectral remote sensing images. Remote Sens. 14 (4), 892.

Wang, P., Wu, P., Song, Y., Hampson, K., Zhong, Y., 2023. A novel spatio-temporally stratified heterogeneity model for identifying factors influencing carbon emissions. Energy Build. 280, 112714.

Wang, J., Zhang, T., Fu, B., 2016. A measure of spatial stratified heterogeneity. Ecol. Indic. 67, 250–256.

Wei, J., Wang, X., 2020. An overview on linear unmixing of hyperspectral data. Math. Probl. Eng. 2020 (5), 1–12.

Wu, Z., Chen, J., Wang, Y., Zhu, Y., Liu, Y., Yao, B., Zhang, Y., Hu, M., 2018. Interactions between water vapor and atmospheric aerosols have key roles in air quality and climate change. Natl. Sci. Rev. 5 (4), 452–454.

Wu, L., Cheng, X., Kang, C., Zhu, D., Huang, Z., Liu, Y., 2020. A framework for mixed-use decomposition based on temporal activity signatures extracted from big geo-data. Int. J. Digit. Earth 13 (6), 708–726.

Xu, D., Chen, R., Xing, X., Lin, W., 2017. Detection of decreasing vegetation cover based on empirical orthogonal function and temporal unmixing analysis. Math. Probl. Eng. 2017.

Xu, D., Fu, M., 2015. Detection and modeling of vegetation phenology spatiotemporal characteristics in the middle part of the Huai River Region in China. Sustainability 7 (3), 2841–2857.

Xu, Y., Huang, B., Xu, Y., Cao, K., Guo, C., Meng, D., 2015. Spatial and temporal image fusion via regularized spatial unmixing. IEEE Geosci. Remote Sens. Lett. 12 (6), 1362–1366.

Xu, X., Li, J., Wu, C., Plaza, A., 2018. Regional clustering-based spatial preprocessing for hyperspectral unmixing. Remote Sens. Environ. 204, 333–346.

Yin, J., Huang, C., Luo, X., Du, Q., 2019. Automatic endmember bundle unmixing methodology for lunar regional area mineral mapping. Icarus 319, 349–362.

Yu, P., Toon, O.B., Bardeen, C.G., Mills, M.J., Fan, T., English, J.M., Neely, R.R., 2015. Evaluations of tropospheric aerosol properties simulated by the community earth system model with a sectional aerosol microphysics scheme. J. Adv. Model. Earth Syst. 7 (2), 865–914.

Zhang, Q., Jimenez, J.L., Canagaratna, M.R., Ulbrich, I.M., Ng, N.L., Worsnop, D.R., Sun, Y., 2011. Understanding atmospheric organic aerosols via factor analysis of aerosol mass spectrometry: a review. Anal. Bioanal. Chem. 401 (10), 3045–3067.

Zhang, L., Li, F., Wei, Q., Yang, X., Wang, W., Yan, M., 2021. Long-term (1975–2016) variations of aerosol optical depth in south central Hebei plain, China, and its correlations with east asian monsoon and economic activities. Arab. J. Geosci. 14 (2), 1–15.

Zhang, Z., Song, Y., Luo, P., Wu, P., 2023. Geocomplexity explains spatial errors. Int. J. Geogr. Inf. Sci. 37 (7), 1449–1469.

Zhang, Z., Song, Y., Wu, P., 2022. Robust geographical detector. Int. J. Appl. Earth Obs. Geoinf. 109, 102782.

Zhang, X., Wang, Y., Niu, T., Zhang, X., Gong, S., Zhang, Y., Sun, J., 2012. Atmospheric aerosol compositions in China: spatial/temporal variability, chemical signature, regional haze distribution and comparisons with global aerosols. Atmos. Chem. Phys. 12 (2), 779–799.

Zhang, X., Wang, H., Xu, S., Yang, Z., 2020. A basic end-member model algorithm for grain-size data of marine sediments. Estuar. Coast. Shelf Sci. 236, 106656.